Wavelet Neural Network Control for Linear Ultrasonic Motor Drive

Faa-Jeng Lin †, *Senior Member*, *IEEE*, Rong-Jong Wai ‡, *Member*, *IEEE* and Po-Kai Huang +

† Department of Electrical Engineering

National Dong Hwa University, Hualien 974, Taiwan

‡ Department of Electrical Engineering

Yuan Ze University, Chung Li 320, Taiwan

+ Department of Electrical Engineering

Chung Yuan Christian University, Chung Li 320, Taiwan

Abstract: A wavelet neural network (WNN) control system is proposed to control the moving table of a linear ultrasonic motor (LUSM) drive system to track periodic reference trajectories in this study. The design of the WNN control system is based on adaptive sliding-mode control technique. First, the structure and operating principle of the LUSM are introduced. Second, since the dynamic characteristics and motor parameters of the LUSM are nonlinear and time-varying, a WNN control system is designed based on adaptive sliding-mode control technique to achieve high-precision position control. In the WNN control system, a WNN is used to learn the ideal equivalent control law, and a robust controller is designed to meet the sliding condition on the sliding surface. The adaptive learning algorithms of the WNN and the bound estimation algorithm of the robust controller are derived from the sense of Lyapunov stability analysis. Finally, the effectiveness of the proposed WNN control system is verified by some experimental results in the presence of uncertainties.

Keywords: Wavelet neural network, Linear ultrasonic motor, Sliding-mode control, Adaptive learning algorithm

I. INTRODUCTION

In recent years, the piezoelectric ceramic motors, which usually operate at ultrasonic frequency, have been widely used in many practical applications due to their merits of smaller dimension, high-holding

force, high force at low speed, silence, no electromagnetic interference and more minimum step size than the classic electromagnetic motors [1]. The basic phenomena of piezoelectric materials permit them to be used as sensors and actuators in a control system. The piezoelectric effects of actuator are usually used to provide linear and rotational motion due to the capability of achieving fine motion without the use of moving mechanical systems. The driving principles of linear ultrasonic motors (LUSMs) are based on the ultrasonic vibration force of piezoelectric ceramic elements and mechanical frictional force [1]. Therefore, their mathematical models are complex [2] and the motor parameters are time-varying due to increasing in temperature and changing in motor drive operating condition [1]; moreover, the control characteristics of the LUSMs are complicated and highly nonlinear. Different constructions and driving principles of LUSMs have been reported [3-6]. They permit high precision, fast control dynamics and large driving force in small dimensions. However, these applications need the detailed mathematical model acquired by complicated modeling process to design control laws in control systems. Besides, the control accuracy is much influenced by the existence of uncertainties, which usually comprises parameter variations, external disturbances and high-order dynamics, etc. In addition, the investigations for the design of drive and control system for LUSM are still poor except that an intelligent position control of a *LC* resonant LUSM drive system was proposed in Lin *et al.* [7]. An unipolar switching full bridge voltage source inverter using *LC* resonant technique was adopted to implement a driving circuit of an LUSM. Moreover, a recurrent fuzzy neural network (RFNN) controller with varied learning rates was investigated to control the moving table of the LUSM to achieve high-precision position control. However, the voltage gain of the *LC* resonant inverter is seriously varied for the variation of quality factor such that the output voltage is different under the same driving frequency. Additionally, the stability of the RFNN control system can not be guaranteed. Therefore, the activation of this study is to deal with the defect of driving circuit and control system for an LUSM in the open literature [7]. Moreover, the driving circuit of the LUSM is a voltage source inverter using *LLCC* resonant technique [8].

In the past years, active research has been carried out in neural network control [9]. The characteristics of fault-tolerance, parallelism and learning suggest that they may be good candidates for implementing real-time adaptive control for nonlinear dynamical systems. It has been proven that artificial neural network can approximate a wide range of nonlinear functions to any desired degree of accuracy under certain conditions [9]. Moreover, much research has been done on applications of

wavelet neural networks, which combine the capability of artificial neural networks in learning from processes and the capability of wavelet decomposition [10-13], for identification and control of dynamic systems [14-17]. In Zhang and Benveniste [14], the new notation of wavelet network was proposed as an alternative to feedforward neural networks for approximating arbitrary nonlinear functions based on the wavelet transform theory. In addition, a backpropagation algorithm was adopted for the training of wavelet network. Zhang et al. [15] described a wavelet-based neural network for function learning and estimation, and the structure of this network is similar to a radial basis function (RBF) network except that the radial functions are replaced by orthonormal scaling functions. From the point of view of function representation, the traditional RBF networks can represent any function that is in the space spanned by the family of basis functions. However, the basis functions in the family are generally not orthogonal and are redundant. It means that the RBF network representation for a given function is not unique and is probably not the most efficient. In this study, the family of basis functions for the RBF network is replaced by an orthogonal basis (i.e., the scaling functions in the theory of wavelets) to form a wavelet neural network [15, 16].

The purpose of this study is to design a wavelet neural network (WNN) control system to control the moving table of a linear ultrasonic motor (LUSM) drive system to track periodic reference trajectories. Moreover, to guarantee the closed-loop stability of the proposed control system, the adaptive sliding-mode control technique [18] is adopted to derive the learning and estimation algorithms in the WNN control system.

II. Linear Ultrasonic Motor

The structure of the SP series LUSM is a large face of a relatively thin rectangular piezoelectric ceramic device as depicted in Fig. 1 [6]. Four electrodes (A, A', B and B') are bounded to the front face to form a checkerboard pattern of rectangles, and each substantially covers one-quarter of this face. The rear face is substantially fully covered with a single electrode. Diagonally located electrodes (A and A'; B and B') are electrically connected by wires. The single electrode on the rear face is grounded via the tuning inductor that can change the resonant frequency. To generate the different moving direction, the electrodes electrified by an AC voltage in the pairs of the diagonal electrodes.

The movement of LUSM is constrained by four support springs with large stiffness. These support springs along a pair of long edges of the LUSM contact the piezoelectric ceramic at points of zero

movement in the *x* direction. A relatively hard ceramic spacer is attached with cement to a short edge of piezoelectric ceramic at the center of the edge. In general, the moving table usually mounts in a V-flat way. A friction force exists on the surface between the moving table and the V-flat way. Besides, it also exists on the contact surface between the moving table and the spacer. In order to transmit the motion of the spacer to the moving table, a preload spring, which is preferably pressed against the middle of a second short edge of piezoelectric ceramic opposite to the short edge with the spacer, is designed to supply pressure between the spacer and the moving table. For a friction drive system, the main efforts contain a normal force, a driving force and a lumped friction force. The normal force is related to the combination of the preload force and the equivalent force of external electric field. Moreover, the driving force of the LUSM, which varies with the trajectory of the spacer, is transmitted to the moving table via the spacer. In addition, the lumped friction force includes the static friction, Coulomb friction and viscous friction, etc. According to the above description, a hypothetical dynamic motion equation can be assumed to take the following form:

$$\ddot{X}(t) = F(X;t) + G(X;t)U(t) + W(X;t) \tag{1}$$

where X is the position of the moving table of the LUSM; $F(X;t)$ denotes a nonlinear dynamic function, which is related to the components of stress, strain and electric field; $G(X;t)$ expresses the control gain of LC resonant inverter; $U(t)$ is the control input, and $W(X;t)$ represents the pre-load force, friction force and unmodelled dynamics in practical applications. Due to the nonlinear and time-varying characteristics of the LUSM, the precise dynamic models are unavailable. Moreover, the LUSM drive system is assumed to be controllable and the sign of $G(X;t)$ is assumed to be positive.

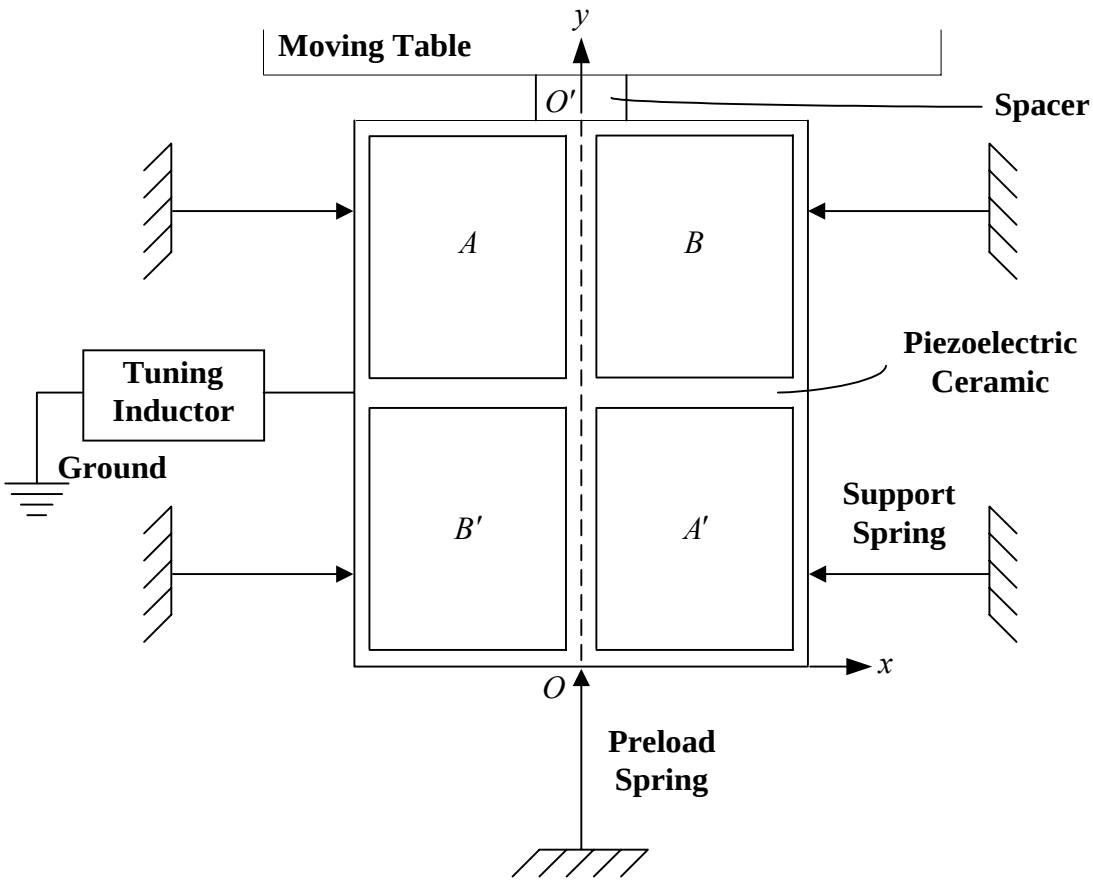

Fig. 1. Structure of LUSM.

III. WAVELET NEURAL NETWORK CONTROL SYSTEM

A four-layer WNN [14, 16] shown in Fig. 2 which is comprised of an input layer (the *i* layer), a wavelet layer (the *j* layer), a product layer (the *k* layer), and an output layer (the *o* layer), is adopted to implement the proposed WNN controller. The inputs of the WNN are r and $r(1-z^{-1})$, in which z^{-1} is a time delay and r is an integral sliding-surface; the output of the WNN is the control input $\hat{U}_{WNN}$. The signal propagation and the basic function in each layer are introduced in the following paragraphs.

For every node *i* in the input layer, the net input and the net output are represented as follows:

$$net_i^1 = x_i^1, \quad y_i^1 = f_i^1(net_i^1) = net_i^1, \quad i = 1, 2 \tag{2}$$

where $x_1^1 = r$ and $x_2^1 = r(1\text{-}z^{-1})$. Moreover, a family of wavelets is constructed by translations and dilations performed on a single fixed function called the mother wavelet. In the wavelet layer each node performs a wavelet ϕ_j that is derived from its mother wavelet. The first derivative of a Gaussian function, $\varphi(x) = -x\exp(-x^2/2)$, is adopted as a mother wavelet in this study. It may be regarded as a differentiable version of the Haar mother wavelet, just as the sigmoid is a differentiable version of a step function, and it has the universal approximation property [16]. For the *j*th node

$$net_j^2 = \frac{y_i^1 - m_{ij}}{\sigma_{ij}}, \quad y_j^2 = f_j^2(net_j^2) = \phi_j(net_j^2), \quad j = 1, \cdots, n \tag{3}$$

where m_{ij} and σ_{ij} are, respectively, the translation and dilation in the *j*th term of the *i*th input y_i^1 to the node of wavelet layer, and *n* is the total number of the wavelets with respect to the input nodes. In addition, each node *k* in the product layer is denoted by $\prod$, i.e., the product of *j* monodimensional wavelets with respect to the input node [16]. For the *k*th rule node

$$net_k^3 = \prod_j w_{jk}^3 y_j^2, \quad y_k^3 = f_k^3(net_k^3) = net_k^3, \quad k = 1, \cdots, l \tag{4}$$

where y_j^2 represents the *j*th input to the node of product layer; w_{jk}^3 represents the weights between the wavelet layer and the product layer and are set to be unity; $l = n/i$ is the number of nodes in product layer if each input node has the same wavelet nodes. Furthermore, the single node *o* in the output layer is labeled as $\sum$, which computes the overall output as the summation of all input signals

$$net_o^4 = \sum_k w_{ko}^4 y_k^3, \quad y_o^4 = f_o^4(net_o^4) = net_o^4, \quad o = 1 \tag{5}$$

where the connecting weight w_{ko}^4 is the output action strength of the *o*th output associated with the *k*th wavelet; y_k^3 represents the *k*th input to the node of output layer; $y_o^4 = \hat{U}_{WNN}$.

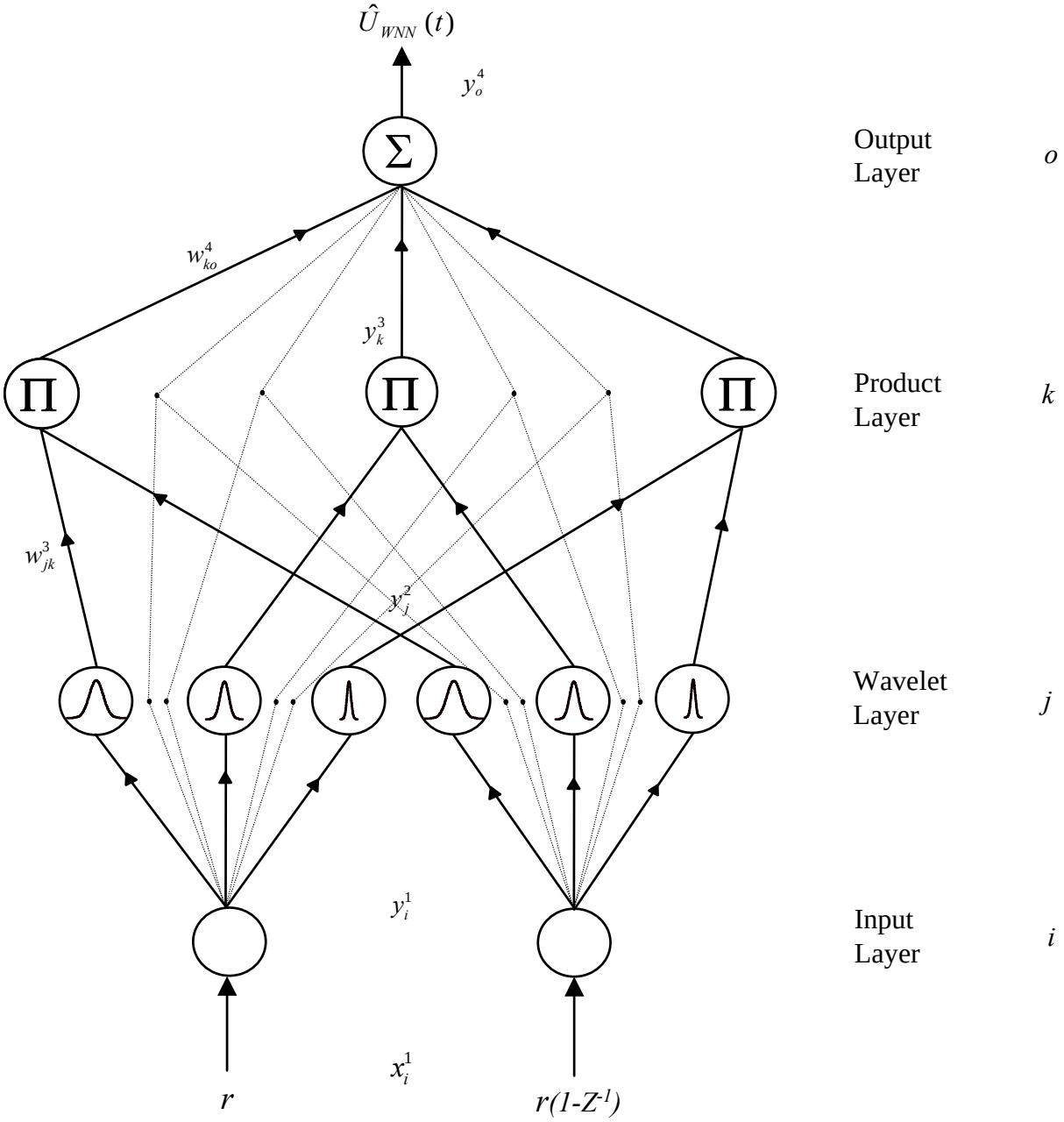

Fig. 2. Structure of WNN.

The control object of this study is to design a WNN control system based on adaptive sliding-mode control technique so that the moving table can track any desired periodic reference trajectories with guaranteed closed-loop stability. To achieve this object, first an integral sliding surface is defined as

$$r(t) = (\frac{d}{dt} + \lambda)^2 \int_0^t e_X(\tau) d\tau \tag{6}$$

where λ is a positive constant; $e_X(t) = X_m(t) - X(t)$ and $X_m(t)$ is the reference trajectory. Differentiate $r(t)$ with respect to time and using (1), the following equation can be obtained

$$\begin{aligned} \dot{r}(t) &= \ddot{e}_X(t) + 2\lambda \dot{e}_X(t) + \lambda^2 e_X(t) \\ &= \ddot{X}_m - F(\mathbf{X};t) - G(\mathbf{X};t)U(t) - W(\mathbf{X};t) + 2\lambda \dot{e}_X(t) + \lambda^2 e_X(t) \end{aligned} \tag{7}$$

Now a control law $U(t)$ is designed to keep the system trajectory on the sliding surface $r(t) = 0$ for $t > 0$. First, the equivalent control $U_{eq}(t)$ is determined by

$$\dot{r}(t)\big|_{U=U_{eq}} = 0 \tag{8}$$

Use (7) and (8) and assume all the system parameters are known, then

$$\ddot{X}_m - F(\mathbf{X};t) - G(\mathbf{X};t)U(t) - W(\mathbf{X};t) + 2\lambda \dot{e}_X(t) + \lambda^2 e_X(t) = 0 \tag{9}$$

The equivalent control can be obtained as follows:

$$U_{eq}(t) = G(X;t)^{-1}[\ddot{X}_m(t) - F(\mathbf{X};t) - W(\mathbf{X};t) + 2\lambda \dot{e}_X(t) + \lambda^2 e_X(t)] \tag{10}$$

Thus, using $\dot{r}(t) = 0$ for $t > 0$, the dynamic in the sliding surface is

$$\ddot{e}_X(t) + 2\lambda \dot{e}_X(t) + \lambda^2 e_X(t) = 0 \tag{11}$$

The desired system dynamics, e.g., the rise-time, overshoot and settling-time, can be easily obtained with the proper selection of λ. However, since the precise dynamic models of the LUSM motion equation are unavailable, (11) is unable to achieve. Moreover, the stability of the closed-loop control system can't be guaranteed. Therefore, the adaptive sliding-mode control technique is adopted in the design of the WNN control system to satisfy both the performance and stability requirements.

According to the structure of the WNN, its output can be represented by the following equation:

$$\hat{U}_{WNN}(r, \boldsymbol{W}, \boldsymbol{m}, \boldsymbol{S}) \equiv \boldsymbol{WQ} \tag{12}$$

where $\mathbf{W} = \left[w_{1o}^4 \cdots w_{ko}^4\right]^T \in \mathbf{R}^{1\times k}$ is the adjustable weights vector in the product-to-output layers; $\mathbf{Q} = \left[y_1^3 \cdots y_k^3\right]^T = \mathbf{Q(P)} = \Theta\mathbf{P}(\mathbf{x_i}) \quad \in \boldsymbol{R}^{k\times 1}$ is the output vector of wavelet layer; $\Theta = \left[w_{1k}^3 \cdots w_{jk}^3\right]^T \in \boldsymbol{R}^{k\times j}$ is the interconnection weights matrix in the wavelet-to-product layer and all the components are set to be one; the first derivative of the Gaussian function $\boldsymbol{P}(\boldsymbol{x_i}) = -(\frac{\boldsymbol{x_i} - \boldsymbol{m}}{\boldsymbol{S}})\exp[-(\frac{\boldsymbol{x_i} - \boldsymbol{m}}{\boldsymbol{S}})^2 / 2] \in \boldsymbol{R}^{j\times 1}$ is adopted as the wavelet functions, in which $\boldsymbol{m} \in \boldsymbol{R}^{j\times 1}$

and $\boldsymbol{S} \in \boldsymbol{R}^{j\times 1}$ are the adjustable parameter vectors of the first derivative of the Gaussian functions; $x_i = [r \quad r(1-z^{-1})]^T \in R^{2\times 1}$ is the input vector of WNN. An optimal WNN controller U^*_{WNN} is designed to learn the idea equivalent control law

$$U_{eq}(t) = U^*_{WNN}(r, \mathbf{W}^*, \mathbf{m}^*, \mathbf{S}^*) + \varepsilon \equiv \mathbf{W}^*\mathbf{Q}^* + \varepsilon \tag{13}$$

where ε is a minimum reconstructed error; $\mathbf{W}^*$, $\mathbf{m}^*$ and $\mathbf{S}^*$ are optimal parameters of $\mathbf{W}$、$\mathbf{m}$ and $\mathbf{S}$. The control law of the WNN control system is designed as follows:

$$U(t) = \hat{U}_{WNN}(r, \hat{\mathbf{W}}, \hat{\mathbf{m}}, \hat{\mathbf{S}}) + U_s \equiv \hat{\mathbf{W}}\hat{\mathbf{Q}} + U_s \tag{14}$$

where $\hat{U}_{WNN}$ is a WNN controller；U_s is a robust controller；$\hat{\mathbf{W}}$、$\hat{\mathbf{m}}$ and $\hat{\mathbf{S}}$ are the adjustable parameters in WNN. The WNN control $\hat{U}_{WNN}$ is used to learn the ideal equivalent control law due to the unknown system dynamics, and the robust control U_s is designed to meet the sliding condition on the sliding surface $r(t) = 0$. Using (1) and (10), the error equation governing the closed-loop system can be obtained:

$$\ddot{e}_X + 2\lambda\dot{e}_X + \lambda^2 e_X = G(X;t)[U_{eq}(t) - U(t)] = \dot{r}(t) \tag{15}$$

Subtracting (14) from (13), the difference between the equivalent control law and the designed control law of the WNN control system can be obtained

$$\tilde{U} = U_{eq} - U = \boldsymbol{W}^*\boldsymbol{Q}^* + \varepsilon - \hat{\boldsymbol{W}}\hat{\boldsymbol{Q}} - U_s = \tilde{\boldsymbol{W}}\boldsymbol{Q}^* + \hat{\boldsymbol{W}}\tilde{\boldsymbol{Q}} + \varepsilon - U_s \tag{16}$$

where $\tilde{\mathbf{W}} = \mathbf{W}^* - \hat{\mathbf{W}}$ and $\tilde{\mathbf{Q}} = \mathbf{Q}^* - \hat{\mathbf{Q}}$. To meet the requirements of closed-loop stability and perfect trajectories tracking, the adaptive learning algorithms for the adjustable parameters of the WNN are derived as follows. The linearization technique is employed to transform the nonlinear wavelet functions into partially linear form so that the expansion of $\tilde{\boldsymbol{Q}}$ in Taylor series is obtained [19, 20]

$$\tilde{\mathbf{Q}} = \Theta\tilde{\mathbf{P}} = \begin{bmatrix} \tilde{p}_1 \\ \tilde{p}_2 \\ \vdots \\ \tilde{p}_j \end{bmatrix} = \Theta \begin{bmatrix} \frac{\partial p_1}{\partial \mathbf{m}} \\ \frac{\partial p_2}{\partial \mathbf{m}} \\ \vdots \\ \frac{\partial p_j}{\partial \mathbf{m}} \end{bmatrix} |_{\mathbf{m}=\hat{\mathbf{m}}} (\mathbf{m}^* - \hat{\mathbf{m}})$$

$$+ \Theta \begin{bmatrix} \frac{\partial p_1}{\partial \mathbf{S}} \\ \frac{\partial p_2}{\partial \mathbf{S}} \\ \vdots \\ \frac{\partial p_j}{\partial \mathbf{S}} \end{bmatrix} |_{\mathbf{S}=\hat{\mathbf{S}}} (\mathbf{S}^* - \hat{\mathbf{S}}) + \Theta\mathbf{O}_\mathbf{n} \tag{17}$$

where $\mathbf{O_n} \in \mathbf{R}^{j\times 1}$ is a vector of the high-order terms of Taylor series. Using the following definitions:

$$\mathbf{P_m} = \left[\frac{\partial p_1}{\partial \mathbf{m}} \quad \frac{\partial p_2}{\partial \mathbf{m}} \quad \cdots \quad \frac{\partial p_j}{\partial \mathbf{m}}\right]^T |_{\mathbf{m}=\hat{\mathbf{m}}} \in \mathbf{R}^{j\times j};$$

$$\mathbf{P_S} = \left[\frac{\partial p_1}{\partial \mathbf{S}} \quad \frac{\partial p_2}{\partial \mathbf{S}} \quad \cdots \quad \frac{\partial p_j}{\partial \mathbf{S}}\right]^T |_{\mathbf{S}=\hat{\mathbf{S}}} \in \mathbf{R}^{j\times j};$$

then (17) can be represented as

$$\tilde{\mathbf{Q}} = \Theta P_{\mathbf{m}} \tilde{\mathbf{m}} + \Theta P_{\mathbf{S}} \tilde{\mathbf{S}} + \Theta \mathbf{O_n} \tag{18}$$

where $\tilde{\mathbf{m}} = \mathbf{m}^* - \hat{\mathbf{m}}$ and $\tilde{\mathbf{S}} = \mathbf{S}^* - \hat{\mathbf{S}}$ are the approximation errors. Equation (18) can be rewritten as

$$\mathbf{Q}^* = \hat{\mathbf{Q}} + \mathbf{Q_m}\tilde{\mathbf{m}} + \mathbf{Q_S}\tilde{\mathbf{S}} + \Theta \mathbf{O_n} \tag{19}$$

where $Q_m = \Theta P_m \in R^{k\times j}$ and $Q_S = \Theta P_S \in R^{k\times j}$. Using (16) and (19), the following equation can be obtained:

$$\begin{aligned}
\tilde{U} &= \mathbf{W}^*\mathbf{Q}^* + \varepsilon - \hat{\mathbf{W}}\hat{\mathbf{Q}} - U_s \\
&= \mathbf{W}^*[\hat{\mathbf{Q}} + \mathbf{Q}_m\tilde{\mathbf{m}} + \mathbf{Q_S}\tilde{\mathbf{S}} + \Theta\mathbf{O_n}] + \varepsilon - \hat{\mathbf{W}}\hat{\mathbf{Q}} - U_s \\
&= (\mathbf{W}^* - \hat{\mathbf{W}})\hat{\mathbf{Q}} + (\tilde{\mathbf{W}} + \hat{\mathbf{W}})\mathbf{Q_m}\tilde{\mathbf{m}} + (\tilde{\mathbf{W}} + \hat{\mathbf{W}})\,\mathbf{Q_S}\tilde{\mathbf{S}} + \varepsilon - U_s + \mathbf{W}^*\Theta\mathbf{O_n} \\
&= \tilde{\mathbf{W}}\hat{\mathbf{Q}} + \hat{\mathbf{W}}\mathbf{Q_m}\tilde{\mathbf{m}} + \hat{\mathbf{W}}\mathbf{Q_S}\tilde{\mathbf{S}} - U_s + \tilde{\mathbf{W}}\mathbf{Q_m}\tilde{\mathbf{m}} + \tilde{\mathbf{W}}\mathbf{Q_S}\tilde{\mathbf{S}} + \mathbf{W}^*\Theta\mathbf{O_n} + \varepsilon \\
&= \tilde{\mathbf{W}}\hat{\mathbf{Q}} + \hat{\mathbf{W}}\mathbf{Q_m}\tilde{\mathbf{m}} + \hat{\mathbf{W}}\mathbf{Q_S}\tilde{\mathbf{S}} - U_s + E
\end{aligned} \tag{20}$$

where the lumped uncertainty term $E = \tilde{\mathbf{W}}\mathbf{Q_m}\tilde{\mathbf{m}} + \tilde{\mathbf{W}}\mathbf{Q_S}\tilde{\mathbf{S}} + \mathbf{W}^*\Theta\mathbf{O_n} + \varepsilon$ is assume to be bounded by $|E| \le \psi$.

THEOREM 1: Consider the LUSM drive system represented by (1). If the control law is designed as (14), in which the adaptive learning algorithms of the WNN controller are designed as (21) ~ (23) and the robust controller is designed as (24) with the adaptive bound estimation shown in (25), then the stability of the proposed WNN control system can be guaranteed.

$$\dot{\hat{\mathbf{W}}} = \eta_1 r(t) G(X;t) \hat{\mathbf{Q}}^T \tag{21}$$

$$\dot{\hat{\mathbf{m}}} = \eta_2 r(t) G(X;t) [\hat{\mathbf{W}}\mathbf{Q_m}]^T \tag{22}$$

$$\dot{\hat{\mathbf{S}}} = \eta_3 r(t) G(X;t) [\hat{\mathbf{W}}\,\mathbf{Q_S}]^T \tag{23}$$

$$U_s = \hat{\psi}(t)\,\mathrm{sgn}(r(t)) \tag{24}$$

$$\dot{\hat{\psi}}(t) = \eta_4 |r(t)| G(X;t) \tag{25}$$

where η_1, η_2, η_3 and η_4 are learning rates which are positive constants; sgn(·) is a sign function; $\hat{\psi}(t)$ is an on-line estimated value of the lumped uncertainty bound ψ.

***Proof*:** Define the approximation error of the uncertainty bound as follows:

$$\tilde{\psi}(t) = \psi - \hat{\psi}(t) \tag{26}$$

Then, the following Lyapunov function candidate is selected

$$L_b = \frac{1}{2} r^2(t) + \frac{1}{2\eta_1} \tilde{\mathbf{W}} \tilde{\mathbf{W}}^T + \frac{1}{2\eta_2} \tilde{\mathbf{m}}^T \tilde{\mathbf{m}} + \frac{1}{2\eta_3} \tilde{\mathbf{S}}^T \tilde{\mathbf{S}} + \frac{1}{2\eta_4} \tilde{\psi}^2(t) \tag{27}$$

Differentiating (27) and using (15) and (20), it is concluded that

$$\begin{aligned}
\dot{L}_b &= r(t)\dot{r}(t) + \frac{1}{\eta_1} \tilde{\mathbf{W}} \dot{\tilde{\mathbf{W}}}^T + \frac{1}{\eta_2} \dot{\tilde{\mathbf{m}}}^T \tilde{\mathbf{m}} + \frac{1}{\eta_3} \dot{\tilde{\mathbf{S}}}^{\mathbf{T}} \tilde{\mathbf{S}} + \frac{1}{\eta_4} \tilde{\psi}(t) \dot{\tilde{\psi}}(t) \\
&= r(t)\, G(X,t)[\tilde{\mathbf{W}} \hat{\mathbf{Q}} + \hat{\mathbf{W}} \mathbf{Q}_{\mathbf{m}} \tilde{\mathbf{m}} + \hat{\mathbf{W}} \mathbf{Q}_{\mathbf{S}} \tilde{\mathbf{S}} - U_s + E] \\
&\quad + \frac{1}{\eta_1} \tilde{\mathbf{W}} \dot{\tilde{\mathbf{W}}}^{\mathbf{T}} + \frac{1}{\eta_2} \dot{\tilde{\mathbf{m}}}^T \tilde{\mathbf{m}} + \frac{1}{\eta_3} \dot{\tilde{\mathbf{S}}}^{\mathbf{T}} \tilde{\mathbf{S}} + \frac{1}{\eta_4} \tilde{\psi}(t) \dot{\tilde{\psi}}(t) \\
&= \tilde{\mathbf{W}}[r(t)\, G(X;t) \hat{\mathbf{Q}} - \frac{1}{\eta_1} \dot{\hat{\mathbf{W}}}^T] + [r(t)\, G(X;t) \hat{\mathbf{W}} \mathbf{Q}_{\mathbf{m}} - \frac{1}{\eta_2} \dot{\hat{\mathbf{m}}}^T] \tilde{\mathbf{m}} \\
&\quad + [r(t) G(X;t) \hat{\mathbf{W}} \mathbf{Q}_{\mathbf{S}} - \frac{1}{\eta_3} \dot{\hat{\mathbf{S}}}^T] \tilde{\mathbf{S}} + r(t)\, G(X;t)[E - U_s] \\
&\quad - \frac{1}{\eta_4} \tilde{\psi}(t) \dot{\hat{\psi}}(t)
\end{aligned} \tag{28}$$

If the adaptation laws of the WNN are chosen as (21) ~ (23) and the robust controller are designed as (24) with the adaptive bound estimation shown in (25), equation (28) can be rewritten as follows:

$$\begin{aligned}
\dot{L}_b &= r(t)\, G(X;t)\, E - r(t)\, G(X;t) \hat{\psi}(t) \operatorname{sgn}(r(t)) - \frac{1}{\eta_4} \tilde{\psi}(t)[\eta_4 |r(t)| G(X;t)] \\
&= r(t)\, G(X;t)\, E - |r(t)| G(X;t) \hat{\psi}(t) - |r(t)| G(X;t)(\psi - \hat{\psi}(t)) \\
&= r(t)\, G(X;t) E - |r(t)| G(X;t) \psi \le |r(t)| G(X;t) |E| - |r(t)| G(X;t) \psi \\
&= |r(t)|\, G(X;t)(|E| - \psi) = -\beta |r(t)|\, G(X;t) \le 0
\end{aligned} \tag{29}$$

Since $\dot{L}_b(r(t), \tilde{\psi}(t), \tilde{\mathbf{W}}, \tilde{\mathbf{m}}, \tilde{\mathbf{S}}) \le 0$, $\dot{L}_b(r(t), \tilde{\psi}(t), \tilde{\mathbf{W}}, \tilde{\mathbf{m}}, \tilde{\mathbf{S}})$ is negative-semidefinite (i.e., $L_b(r(t), \tilde{\psi}(t), \tilde{\mathbf{W}}, \tilde{\mathbf{m}}, \tilde{\mathbf{S}}) \le L_b(r(0), \tilde{\psi}(0), \tilde{\mathbf{W}}, \tilde{\mathbf{m}}, \tilde{\mathbf{S}})$), which implies $r(t)$、$\tilde{\psi}(t)$、$\tilde{\mathbf{W}}$、$\tilde{\mathbf{m}}$ and $\tilde{\mathbf{S}}$ are bounded. Let function $\Xi(t) \equiv \beta\, |r(t)| G(X;t) \le -\dot{L}_b$, and integrate $\Xi(t)$ with respect to time

$$\int_0^t \Xi(\tau)\, d\tau \le L_b(r(0), \tilde{\psi}(0), \tilde{\mathbf{W}}, \tilde{\mathbf{m}}, \tilde{\mathbf{S}}) - L_b(r(t), \tilde{\psi}(t), \tilde{\mathbf{W}}, \tilde{\mathbf{m}}, \tilde{\mathbf{S}}) \tag{30}$$

Because $L_b(r(0), \tilde{\psi}(0), \tilde{\mathbf{W}}, \tilde{\mathbf{m}}, \tilde{\mathbf{S}})$ is bounded and $L_b(r(t), \tilde{\psi}(t), \tilde{\mathbf{W}}, \tilde{\mathbf{m}}, \tilde{\mathbf{S}})$ is nonincreasing and bounded, the following result is obtained

$$\lim_{t \to \infty} \int_0^t \Xi(\tau)\, d\tau < \infty \tag{31}$$

It can be concluded that $\dot{\Xi}(t)$ is bounded, and $\Xi(t)$ is uniformly continuous. Using Barbalat's Lemma

[21, 22], it can be shown that $\lim_{t\to\infty}\Xi(t)=0$. Thus, $r(t)\to 0$ as $t\to\infty$. As a result, the stability of the proposed WNN control system can be guaranteed. *Q.E.D.*

According to the unavailable system states, the $G(X;t)$ in the tuning algorithms is reorganized as $|G(X;t)|\text{sgn}(G(X;t))$ in practical applications. Therefore, the adaptive laws for the proposed WNN control system shown in (21) ~ (23) and (25) can be reorganized as follows:

$$\dot{\hat{\mathbf{W}}}=\alpha_1 r(t)\,\text{sgn}(G(X;t))\,\hat{\mathbf{Q}}^T \tag{32}$$

$$\dot{\hat{\mathbf{m}}}=\alpha_2 r(t)\,\text{sgn}(G(X;t))[\hat{\mathbf{W}}\mathbf{Q_m}]^T \tag{33}$$

$$\dot{\hat{\mathbf{S}}}=\alpha_3 r(t)\,\text{sgn}(G(X;t))[\hat{\mathbf{W}}\mathbf{Q_S}]^T \tag{34}$$

$$\dot{\hat{\psi}}(t)=\alpha_4 |r(t)|\,\text{sgn}(G(X;t)) \tag{35}$$

where the terms $\eta_i|G(X;t)|$ are absorbed by the learning-rate parameters or the adaptation gains α_i, which are some positive constant to be determined. Consequently, only the sign of $G(X;t)$ is required in the design procedure, and it can be easily obtained from the physical characteristic of the controlled system. The proposed WNN control system is shown in Fig. 3.

IV. PC-Based LUSM Drive and Experimental Results

The adopted LUSM is SP-2 with 10W 270Vrms 0.14Arms 8N. A servo control card is installed in PC-based control computer [7], which includes multi-channels of D/A, A/D, PIO and encoder interface circuits. The position of the moving table is fed back using a linear scale. Digital filters and frequency multiplied by 4 circuits are built into the encoder interface circuits to increase the precision of position feedback. The resulted resolution is $1\,\mu$m. The proposed WNN control system is realized in the Pentium using the "Turbo C" language. The control interval of the WNN control system is set at 1msec. The amplitude of the DC-link voltage is controlled by the push-pull DC/DC converter [8] in which the output of the WNN control system, $U(t)$, is used as the pulse-width-modulation (PWM) control voltage for the push-pull DC/DC converter. The output of the *LLCC* resonant tank [8] is a high voltage sinusoidal wave operating at the geometric frequency, and the amplitude is proportional to the variable amplitude control. The high voltage sinusoidal wave is applied to electrode pair *A*, *A′* or *B*, *B′* as shown in Fig. 1 to move the moving table in the desired direction. Two test conditions are provided in the experimentation, which are the nominal case and the parameter variation case. The parameter variation case is the addition of one iron disk with 3.7kg weight on the moving table.

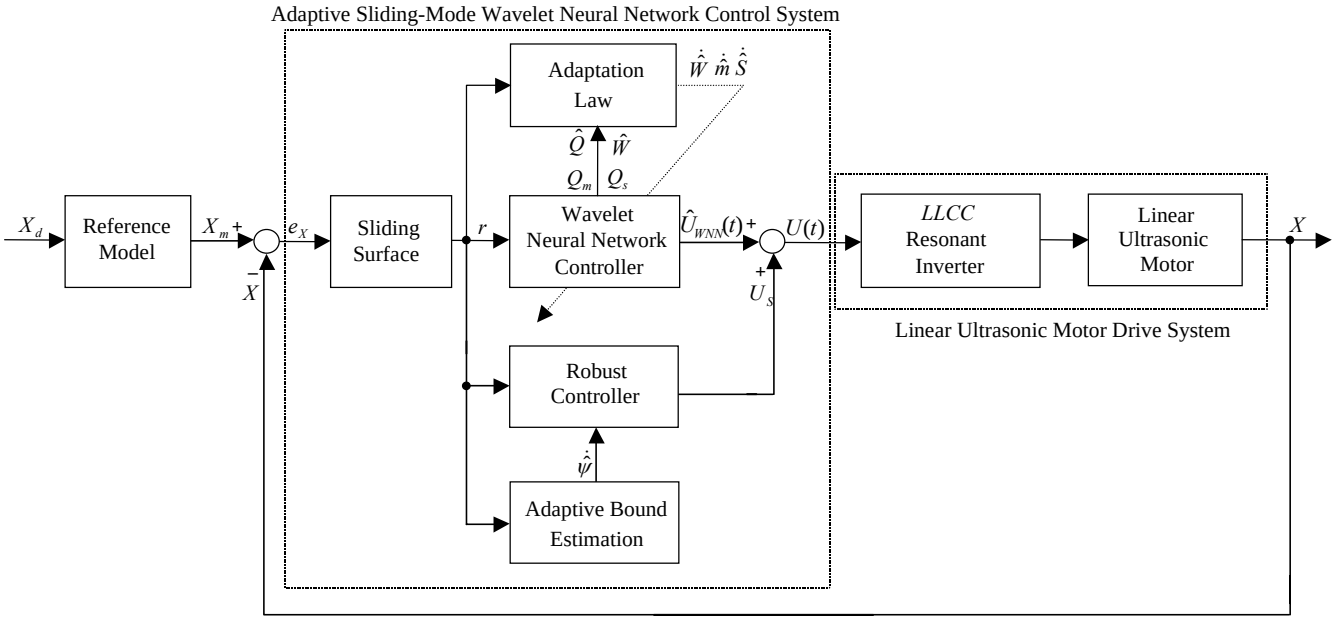

Fig. 3. Block diagram of WNN control system.

To show the effectiveness of the WNN control with small rule set, the WNN has two, fourteen, seven and one neurons at the input, wavelet, product and output layers, respectively. The λ in the sliding surface is set at 0.5. Moreover, a 2nd-order transfer function of the following form with rise time 0.3sec is chosen as the reference model for the periodic step command:

$$\frac{\omega_n^2}{s^2+2\zeta\omega_n s+\omega_n^2}=\frac{168.1}{s^2+25.93s+168.1} \tag{36}$$

where s is the Laplace operator; ζ and ω_n are the damping ratio (set at one for critical damping) and undamped natural frequency. When the command is a sinusoidal reference trajectory, the reference model is set to be one. The control objective is to control the moving table to move 2.5cm periodically for periodic step command and to move $\pm$2.5cm periodically for periodic sinusoidal command.

All the gains in the adaptive laws of the WNN control system should be chosen to achieve the best control performance in the experimentation considering the limitation of control effort, the requirement of stability and the possible operating conditions. The following adaptation gains are chosen for various test condition:

$$\alpha_1=12、\ \alpha_2=4、\ \alpha_3=4 \text{ and } \alpha_4=0.001 \tag{37}$$

The experimental results due to periodic step and sinusoidal commands at the nominal case using the adaptation gains shown in (37) are depicted in Fig. 4. The tracking response, tracking error $e_X(t)$ and control effort $U(t)$ for periodic step command are depicted in Figs. 4(a), 4(b) and 4(c). The tracking response, tracking error $e_X(t)$ and control effort $U(t)$ due to periodic sinusoidal command are given in Figs. 4(d), 4(e) and 4(f). From the experimental results, good tracking responses can be obtained and the tracking errors converge quickly, and the chattering phenomena do not exist in the control efforts for various reference trajectories with properly selected adaptation gains.

To further test the robust control performance of the proposed WNN control system, the experimental results for the parameter variation case using the adaptation gains (37) with adaptive bound estimation are shown in Fig. 5. The tracking response, tracking error $e_X(t)$ and control effort $U(t)$ for periodic step command are depicted in Figs. 5(a), 5(b) and 5(c). The tracking response, tracking error $e_X(t)$ and control effort $U(t)$ due to periodic sinusoidal command are given in Figs. 5(d), 5(e) and 5(f). From the experimental results, the tracking errors converge quickly, and the robust control characteristics of the proposed WNN control scheme under the occurrence of uncertainties for various reference trajectories can be clearly observed.

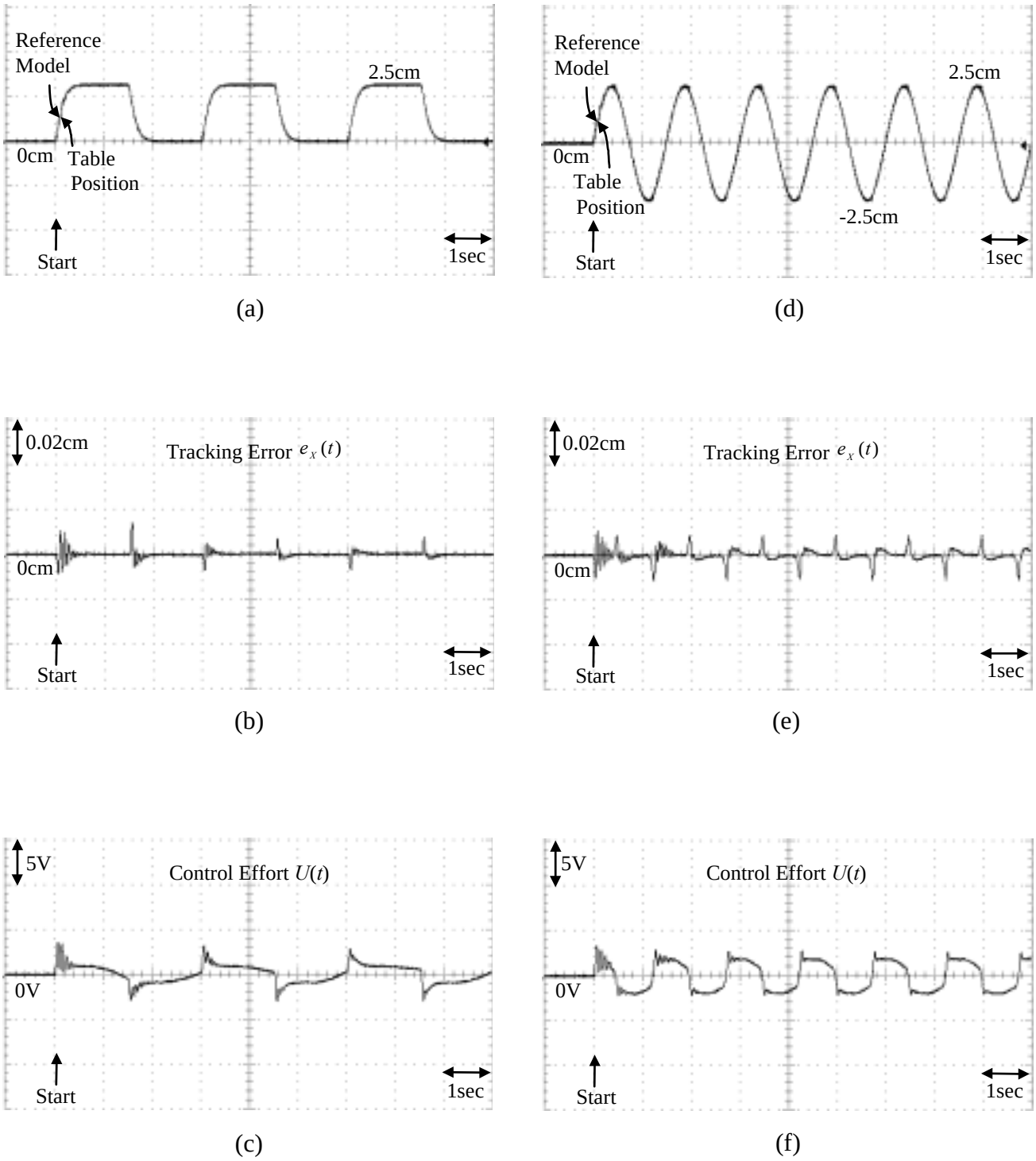

Fig. 4. Experimental results of WNN control system with adaptive lumped uncertainty bound at nominal case: (a), (b), (c) tracking response, tracking error $e_X(t)$, and control effort $U(t)$ due to periodic step command; (d), (e), (f) tracking response, tracking error $e_X(t)$, and control effort $U(t)$ due to periodic sinusoidal command.

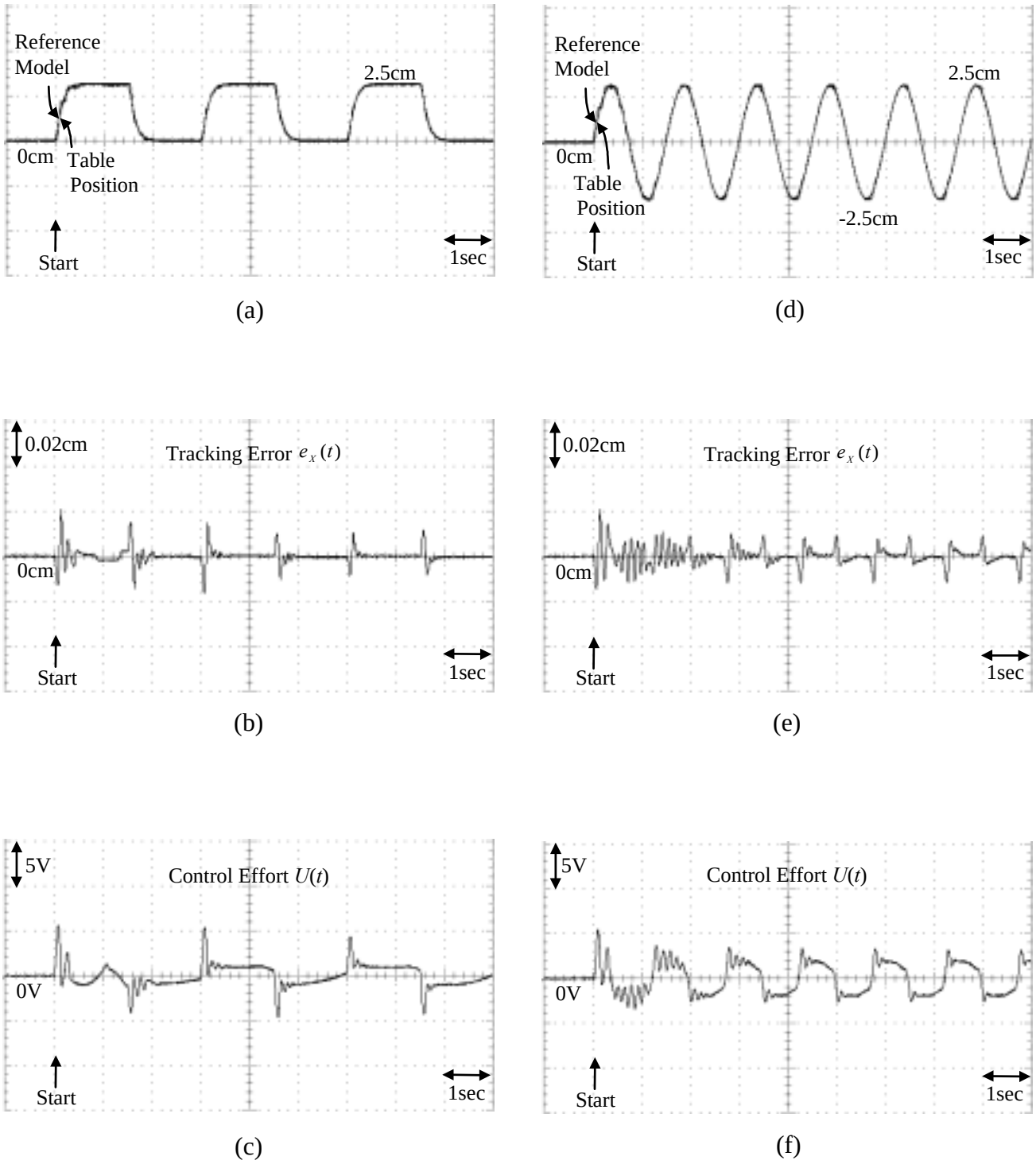

Fig. 5. Experimental results of WNN control system with adaptive lumped uncertainty bound at parameter variation case: (a), (b), (c) tracking response, tracking error $e_X(t)$, and control effort $U(t)$ due to periodic step command; (d), (e), (f) tracking response, tracking error $e_X(t)$, and control effort $U(t)$ due to periodic sinusoidal command.

V. CONCLUSIONS

The dynamic characteristics of the LUSM are nonlinear and time-varying and the precise dynamic model is difficult to obtain. Therefore, a WNN control system has been proposed to control the position of the moving table of the LUSM to achieve high-accuracy position control via the adaptive sliding-mode control technique in this study. In the WNN control system, a WNN is used to learn the ideal equivalent control law, and a robust controller is designed to meet the sliding condition on the sliding surface. All the adaptive laws in the WNN control system are derived in the sense of Lyapunov stability analysis, thus, the system-tracking stability can be guaranteed in the closed-loop system. Moreover, no constrained conditions and prior knowledge of the controlled system are required in the design process. To verify the effectiveness of the proposed control scheme, the WNN control system is implemented in a PC-based computer control system, and the LUSM is driven by a voltage source inverter using *LLCC* resonant technique. From the experimental results, the position tracking responses of the moving table can be controlled to closely follow the reference trajectories under various operating conditions.

ACKNOWLEDGMENT

The authors would like to acknowledge the financial support of Energy & Resources Labs., Industrial Technology Research Institute, Taiwan, R.O.C. through grant number 3000015324.

REFERENCE

[1] T. Sashida and T. Kenjo, *An Introduction to Ultrasonic Motors*. Oxford: Clarendon Press, 1993.

[2] N. W. Hagood and A. J. Mcfarland, “Modeling of a piezoelectric rotary ultrasonic motor,” *IEEE Trans. Ultrason., Ferroelect., and Freq. Cont.,* vol. 42, no. 2, pp. 210-224, 1995.

[3] Y. Tomikawa, T. Takano, and H. Umeda, “Thin rotary and linear motors using a double-mode piezoelectric vibrator of the first longitudinal and second bending modes,” *Jpn. J. Appl. Phys.*, vol. 31, pt. 1, no. 9B, pp. 3073-3076, 1992.

[4] M. Aoyagi and Y. Tomikawa, “Ultrasonic motors using longitudinal and bending multimode vibrators with mode coupling caused by external additional asymmetry,” *Jpn. J. Appl. Phys.*, vol. 32, pt. 1, no. 9B, pp. 4190-4193, 1993.

[5] M. Kummel, S. Goldschmidt, and J. Wallaschek, “Theoretical and experimental studies of a

piezoelectric ultrasonic linear motor with respect to damping and nonlinear material behavior," *Ultrasonics*, vol. 36, pp. 103-109, 1998.

[6] J. Zumeris, *Ceramic Motor*. *United States Patent, 5777423,* 1998.

[7] F. J. Lin, R. J. Wai, K. K. Shyu, and T. M. Liu, "Recurrent fuzzy neural network control for piezoelectric ceramic linear ultrasonic motor drive," *IEEE Tran. Ultra. Ferro. Freq. Ctrl.*, vol. 48, no. 4, pp. 900-913, 2001.

[8] F. J. Lin, R. Y. Duan, R. J. Wai, and C. M. Hong, "LLCC resonant inverter for piezoelectric ultrasonic motor drive," *IEE Proc.-Electr. Power Appl.*, vol. 146, no. 5, pp. 479-487, 1999.

[9] O. Omidvar and D.L. Elliott, *Neural Systems for Control*. Academic Press, 1997.

[10] Y. C. Pati and P. S. Krishnaprasad, "Analysis and synthesis of feedforward neural networks using discrete affine wavelet transformations," *IEEE Trans. Neural Netw*., vol. 4, no. 1, pp. 73-85, 1993.

[11] B. Delyon, A. Juditsky, and A. Benveniste, "Accuracy analysis for wavelet approximations," *IEEE Trans. Neural Netw*., vol. 6, no. 2, pp. 332-348, 1995.

[12] C. F. Chen and C. H. Hsiao, "Wavelet approach to optimising dynamic systems," *IEE Proc. Control Theory Appl*., vol. 146, no. 2, pp. 213-219, 1999.

[13] T. Lindblad and J.M. Kinser, "Inherent features of wavelets and pulse coupled networks," *IEEE Trans. Neural Netw*., vol. 10, no. 3, pp. 607-614, 1999.

[14] Q. Zhang and A. Benveniste, "Wavelet networks," *IEEE Trans. Neural Netw*., vol. 3, no. 6, pp. 889-898, 1992.

[15] J. Zhang, G. G. Walter, Y. Miao and W. N. W. Lee, "Wavelet neural networks for function learning," *IEEE Trans. Signal Processing*, vol. 43, no. 6, pp. 1485-1496, 1995.

[16] Y. Qussar, I. Rivals, L. Personnaz, and G. Dreyfus, "Training wavelet networks for nonlinear dynamic input–output modeling," *Neurocomputing*, vol. 20, pp. 173-188, 1998.

[17] L. M. Reyneri, "Unification of neural and wavelet networks and fuzzy systems," *IEEE Trans. Neural Netw*., vol. 10, no. 4, pp. 801-814, 1999.

[18] F. J. Lin and S. L. Chiu, "Adaptive fuzzy sliding mode control for PM synchronous servo motor drive," *IEE Proc.- Control Theory Appl.*, vol. 145, no. 1, pp. 63-72, 1998.

[19] Y. G. Leu, T. T. Lee, and W. Y. Wang, "Observer-based adaptive fuzzy-neural control for unknown nonlinear dynamical systems," *IEEE Trans. Syst., Man, and Cybern.*, vol. 29, no. 5, pp.

583-591, 1999.

[20] Y. G. Leu, W. Y. Wang, and T. T. Lee, “Robust adaptive fuzzy-neural controllers for uncertain nonlinear systems,” *IEEE Trans. Robotics and Automation*, vol. 15, no. 5, pp. 805-817, 1999.

[21] J. -J. E. Slotine and W. Li, *Applied Nonlinear Control*. Prentice-Hall, New Jersey, 1991.

[22] K. J. Astrom and B. Wittenmark, *Adaptive Control*. Addison-Wesley, New York, 1995.